NANO LETTERS

Letter

pubs.acs.org/NanoLett

Engineering Light Outcoupling in 2D Materials

Der-Hsien Lien,[†,‡,§,∥,▽] Jeong Seuk Kang,[†,‡,▽] Matin Amani,[†,‡] Kevin Chen,[†,‡] Mahmut Tosun,[†,‡] Hsin-Ping Wang,[†,‡,§,∥] Tania Roy,[†,‡] Michael S. Eggleston,[†] Ming C. Wu,[†] Madan Dubey,[⊥] Si-Chen Lee,[∥] Jr-Hau He,*[,§] and Ali Javey*[,†,‡]

[†]Electrical Engineering and Computer Sciences, University of California, Berkeley, California 94720, United States

[‡]Materials Sciences Division, Lawrence Berkeley National Laboratory, Berkeley, California 94720, United States

[§]Computer, Electrical and Mathematical Sciences and Engineering (CEMSE) Division, King Abdullah University of Science & Technology (KAUST), Thuwal 23955-6900, Saudi Arabia

[∥]Department of Electrical Engineering, Institute of Electronics Engineering, National Taiwan University, Taipei 10617, Taiwan, Republic of China

[⊥]Sensors and Electron Devices Directorate, U.S. Army Research Laboratory, Adelphi, Maryland 20783, United States

Supporting Information

ABSTRACT: When light is incident on 2D transition metal dichalcogenides (TMDCs), it engages in multiple reflections within underlying substrates, producing interferences that lead to enhancement or attenuation of the incoming and outgoing strength of light. Here, we report a simple method to engineer the light outcoupling in semiconducting TMDCs by modulating their dielectric surroundings. We show that by modulating the thicknesses of underlying substrates and capping layers, the interference caused by substrate can significantly enhance the light absorption and emission of WSe_2, resulting in a ~11 times increase in Raman signal and a ~30 times increase in the photoluminescence (PL) intensity of WSe_2. On the basis of the interference model, we also propose a strategy to control the photonic and optoelectronic properties of thin-layer WSe_2. This work demonstrates the utilization of outcoupling engineering in 2D materials and offers a new route toward the realization of novel optoelectronic devices, such as 2D LEDs and solar cells.

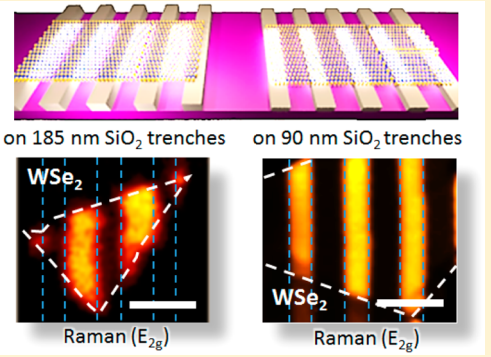

KEYWORDS: *2D materials, light outcoupling, substrate interference, photoluminescence, Raman*

Atomically thin two-dimensional (2D) transition metal dichalcogenides (TMDCs), such as MoS_2 and WSe_2, have recently positioned themselves as strong candidates for future optoelectronics.[1−5] When assessing the optical, electronic, and structural properties of these materials, micro-Raman and photoluminescence (PL) spectroscopies are often considered as quick and nondestructive methods. These techniques allow for the emission intensity and the peak energy position of emitted photons to be examined, which provide an informative matrix for evaluating the quality of materials.[6−8] Previously, it has been demonstrated that suspending the 2D materials can enhance the resolution of their optical signals. For example, suspended graphene and MoS_2 have shown enhanced PL/Raman signals, which are attributed to the diminishment of detrimental interactions between the materials and substrates, such as nonradiative recombination, charge transfer, and excitonic transitions.[9−13] On the other hand, the dielectric surroundings around the atomically thin 2D materials could optically regulate the incoupling and outcoupling of light, yielding a dramatic variation of the emission intensity.[14−17] However, the effect has not been explored in detail and is often overlooked. In this study, we show that the PL/Raman emission intensity of suspended 2D materials could be either enhanced or suppressed depending on the thickness of the underlying substrates or the depth of the trenches for suspended samples. Through modeling and experiments, we comprehensively investigate the roles of underlying substrates and surface coatings and their optical interference effects on TMDCs. By modulating the thickness of underlying substrates and capping layers, the absorption and emission of light can be engineered, giving tunable PL and Raman intensities by up to 11 and 30 times, respectively. Our results suggest an extremely simple way to significantly enhance the outcoupling of thin-layer TMDCs, which is crucial for optoelectronic devices built with semiconducting TMDCs, such as 2D LEDs, lasers and photonic components. Most notably, the concept enables the control of 2D materials' photonic properties, which provides design criteria for their photonic and optoelectronic components.

In an effort to improve the light−matter interaction, incorporating plasmonics and microcavities with 2D materials

Received: December 2, 2014
Revised: January 14, 2015

DOI: 10.1021/nl504632u
Nano Lett. XXXX, XXX, XXX−XXX

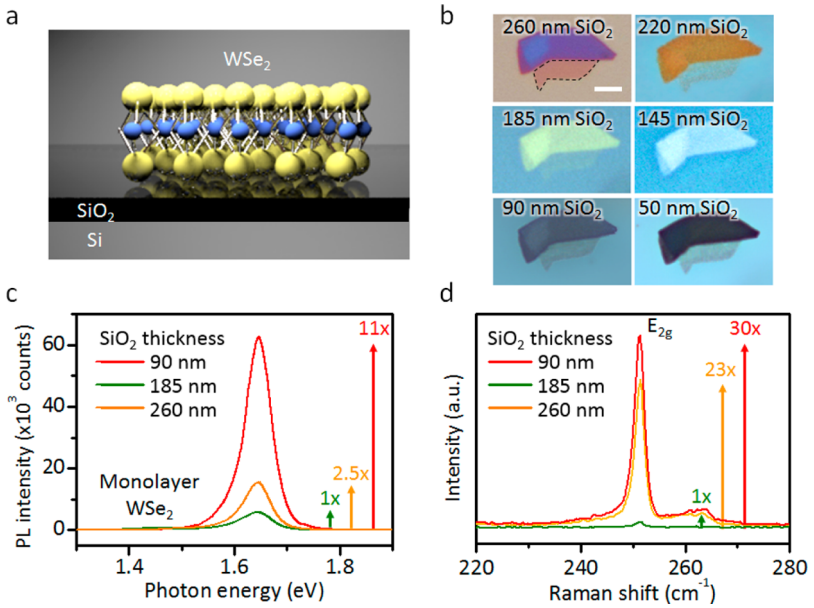

Figure 1. (a) Schematic of a single-layer WSe_2 on a SiO_2/Si substrate. (b) Optical images of a WSe_2 flake transferred onto SiO_2/Si substrates with different SiO_2 thicknesses. The white scale bar in the figure indicates 10 μm. (c) PL and (d) Raman spectra of WSe_2 flakes on substrates with 90, 185, and 260 nm SiO_2.

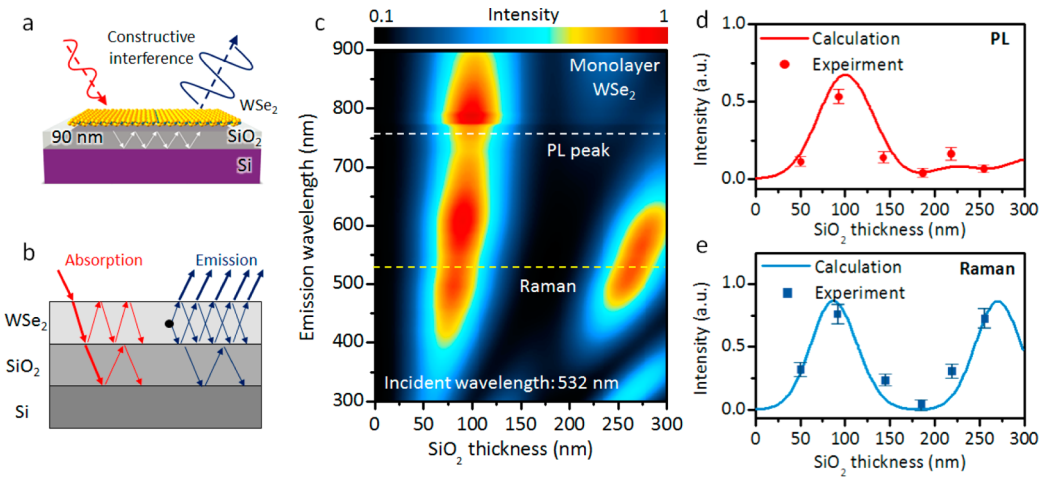

Figure 2. (a) Illustration of the outcoupling mechanism considering absorption and emission of light. (b) Illustration of the multiple reflections within the structure and the optical paths for absorption and emission processes. (c) Intensity map for light outcoupling as a function of both the emission wavelength and the SiO_2 thickness. Experimental and calculation results of (d) PL (at 752 nm) and (e) Raman (532 nm) scattering intensities.

has proven to be viable for facilitating the light incoupling so as to achieve improved absorption.[18−20] Another intuitive approach improved the interaction by modifying the dielectric surrounding of TMDCs.[15,16] Substrate interference has been applied in the past as a simple way to precisely quantify the thickness of SiO_2 films grown on Si substrates by evaluating its reflection color.[21] Such effects have also been used to tune the contrast/visibility/color of graphene and MoS_2 on Si/SiO_2 substrates, which allows monolayers to be seen and thicknesses to be identified under an optical microscope.[22,23] Here, we demonstrate that engineering substrate interferences can be also used to enhance the light outcoupling of 2D materials, which is applicable to all 2D materials systems. WSe_2 is used for this demonstration because of its distinct PL and Raman responses and its well-studied optical properties. WSe_2 flakes were prepared by micromechanical exfoliation and characterized by atomic force microscopy to identify the number of atomic layers (NL) of each flake. Then the flakes were transferred onto different substrates using poly(methyl methacrylate) (PMMA) as the transfer medium.[24] Figure 1a and b present the aforementioned schematic and optical images of a WSe_2 flake transferred on SiO_2/Si substrates with different SiO_2 thicknesses. When sitting on different substrates, the color contrast of the monolayer WSe_2 shows apparent differences, indicating the interference between the substrate and flake is wavelength-dependent. Theses color changes also imply that the light output intensity can vary with respect to the emission wavelengths. To verify these phenomena, we examine the PL and Raman spectra of the same monolayer WSe_2 on different substrates, as shown in Figure 1c and d. For PL measurements, peak values are at 1.65 eV, corresponding to the bandgap of WSe_2 monolayers.[6,25] In addition, the Raman peak at ∼250

DOI: 10.1021/nl504632u
Nano Lett. XXXX, XXX, XXX−XXX

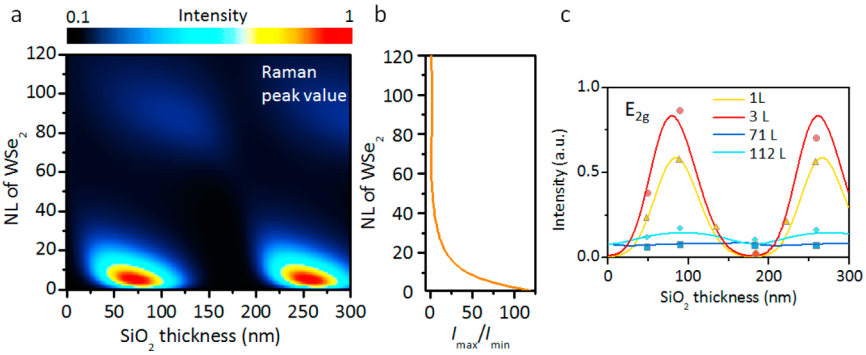

Figure 3. (a) Calculation of the thickness-dependent Raman intensities for WSe_2. (b) Enhancement ratio (I_{max}/I_{min}) extracted from the relative intensity map. (c) Calculation and experimental results for WSe_2 as a function of NL.

cm^{-1}, corresponding to the E_{2g} in-plane atomic vibration mode, is examined in this study. Note that all samples performed in this study were carried out under identical measurement conditions (see Methods). Due to the different emission wavelengths for PL and Raman measurements, their enhancements depend differently on SiO_2 thickness. The PL intensity of WSe_2 on 90 nm SiO_2 is enhanced the most, by 11 times, when compared to its PL on 185 nm SiO_2, whereas its Raman signal is enhanced the most, by 30 times, on 260 nm SiO_2 substrates. Note that the intensity change is reversible, as demonstrated by transferring the flake back onto the previous substrates (Supporting Information Figure S1). Here, sample-to-sample variation could be eliminated because the dry-transfer method used allowed for the same flake to be measured. We also show that the Raman intensity changes without a measurable peak shift, indicating that strain does not play a significant role in these results.[6]

The enhancement of light outcoupling assisted by substrate-induced light interferences can be explained simply by employing the multiple reflection model, as shown in Figure 2a and b.[25,26] Considering multiple interfaces in this structure, incident light will encounter the boundaries of PMMA/WSe_2, Wse_2/SiO_2, and SiO_2/Si, undergoing multiple reflections. The four media, including PMMA, WSe_2, SiO_2, and Si, are denoted as i = 0, 1, 2, and 3, respectively (Figure 2b). As both the absorption and emission are taken into account, the intensity of light outcoupled from the WSe_2 layer can be deduced as

$$I = \int_0^d |E_{ab}(x)E_{em}(x)|^2 \, dx$$

where d is the thickness of the flake, and $E_{ab}(x)$ and $E_{em}(x)$ are the electric field amplitudes within the flakes and light emitting out the flakes, respectively (Supporting Information S2). Note that according to previous reports,[16] the oblique incidence caused by the objective (numerical aperture = 0.9) will only lead to minute changes in the spectral response, so the assumption of a majority of normal incidence is still valid. We also note that this simplified model was used before to design substrates that increase the optical contrast between graphene and MoS_2.[16,26]

On the basis of the multiple reflection model, we are able to create a two-dimensional map quantifying the light outcoupling strength as a function of both the emission wavelength and SiO_2 thickness, as shown in Figure 2c. Here, the map presents the emission wavelength ranging from 300 to 900 nm and the SiO_2 thickness ranging from 0 to 300 nm. As shown in Figure 2d and e, the intensity at 752 nm (1.65 eV; direct bandgap emission of monolayer WSe_2) and 532 nm are specified, which correspond to the PL emission and Raman scattering wavelengths of WSe_2, respectively. For PL emission, the maximum intensity is seen at a SiO_2 thickness of ~90 nm. For Raman scattering, the maxima are at ~90 and 260 nm SiO_2 thicknesses. Those are in good agreement with the experimental results shown in Figure 1c and d. Note that changing the incident wavelength will produce a new set of light outcoupling maps based on the equations provided in the supplementary. The improved outcoupling is attributed to a combined effect of enhanced absorption and emission modulated by substrate-induced interference (Supporting Information Figure S3). Because the incident light is fixed (532 nm), the amount of light absorption is mainly governed by the Fabry–Perot interference, which shows a periodic variance with SiO_2 thickness. On the other hand, the strength of emission shows an irregular profile due to the combined effects of substrate interference and the wavelength-dependent refractive index. Enhanced outcoupling occurs when both absorption and emission meet constructive interference, which yields ~11 times enhancement of PL and 30 times enhancement of Raman compared to those in destructive cases.

The thickness of WSe_2 also has an effect on light outcoupling. Figure 3a shows a calculated Raman intensity map as a function of WSe_2 NL and SiO_2 thickness. For thinner flakes (NL < 10), two enhancement regions are located at the thicknesses of ~90 and 260 nm, corresponding to the constructive interference as mentioned above. To highlight the interference–NL dependence, the enhancement ratio (I_{max}/I_{min}) is plotted as shown in Figure 3b, where I_{max} and I_{min} are the maximum and minimum intensities, respectively, within the range defined in this map (SiO_2 thickness from 0 to 100 nm and NL from 1 to 120 L). The curve demonstrates that the enhancement becomes pronounced as the number of layers is reduced. For instance, the ratio for monolayer WSe_2 is over 100, whereas for the thicker flakes (NL > 30) the substrate effect is almost diminished (enhancement ratio <2). To compare the simulated maps with experiments, we measured the Raman (E_{2g}) intensity of 1, 3, 71, and 121 layers thick flakes on different substrates, as shown in Figure 3c. The NL of the flakes is obtained by AFM and then the flakes are transferred onto different substrates via the same technique described above. For NL = 1 and 3, the response shows apparent variance with changing SiO_2 thickness, whereas for NL = 71 and 121 the SiO_2 thickness dependence becomes weak. The results demonstrate that thinner layers are more sensitive to the substrate effect, agreeing well with the calculation shown in

DOI: 10.1021/nl504632u
Nano Lett. XXXX, XXX, XXX–XXX

Figure 3b. Note that the same effect is also valid for PL responses though a direct to indirect transition with increasing layers dominates the PL intensity rather than the substrate effect (see Supporting Information Figure S4).

From finite-difference time-domain (FDTD) simulations shown in Figure 4, a concentrated electric field is observed at

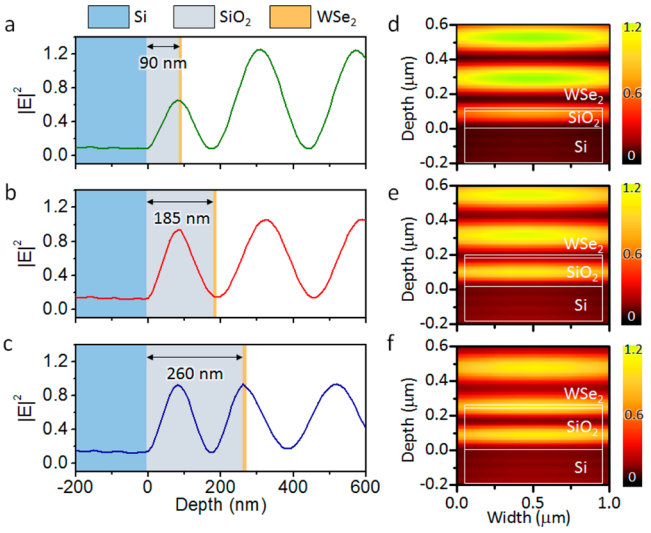

Figure 4. (a, b, c) Intensity of light as a function of penetration depth for different SiO_2 substrate thicknesses. (d, e, f) Intensity map for different SiO_2 substrate thicknesses. Note that the incident light comes from the top and the incident wavelength is 532 nm, corresponding to the experimental conditions. The depths at which Si, SiO_2, and WSe_2 are located are marked in the figures as white boxes.

the surfaces of 90 and 260 nm SiO_2 substrates, indicating that standing waves are formed. On the other hand, a valley of intensity is observed at the surface of a 185 nm SiO_2 substrate. The effect of the double layer structure is similar to a resonant cavity where a reflecting Si surface with a transparent SiO_2 layer can be regarded as a half cavity. When the substrate thickness equals a quarter the wavelength of incident light, the substrates provides constructive interference to facilitate the incoupling of light to flakes. It also shows that as the substrate thickness is varied, the electrical intensity within thinner WSe_2 (smaller window) will experience a more dramatic variation than the thicker WSe_2 (smaller window). Such a substrate effect will be minimized as the 2D materials become thicker than a quarter wavelength ($d = \lambda/4n$; d = ~26 nm corresponding to NL = 37),[14] in accordance with the observations shown in Figure 3. Recently, rise of advanced techniques in Raman spectroscopy, such as tip-enhanced Raman spectroscopy (TERS) and surface-enhanced Raman spectroscopy (SERS), have provided the ability to better resolve the absorbances, defects, and heterojunctions of 2D systems.[27] Compared to those techniques, this work provides an alternative strategy, namely, substrate-enhanced Raman spectroscopy, to achieve higher resolution for 2D materials characterization simply by adjusting the substrate (see Supporting Information Figure S5).

In addition to being used for materials characterization, this technique can be also used for controlling the photonic properties of 2D materials, which paves a new way for the fabrication of 2D photonic components. As an example, Figure 5 shows that the light outcoupling of WSe_2 can be locally engineered by manipulating the refractive index of the substrates. To modify the substrates, electron-beam lithography is used to define periodic trenches on SiO_2/Si substrates. The SiO_2 layer in the trenches is fully etched so that the depth of the trenches are the same as the thicknesses of the SiO_2 layer. Here, substrates with 90 and 185 nm SiO_2 are used, which correspond to the most constructive and destructive substrates, respectively. Due to the difference of refractive indices between the SiO_2 (n = 1.46) and air (n = 1), the substrate forms a discrete refractive index variance along the surface. Figure 5a and b show the optical and Raman mapping images of the WSe_2 flakes after they were transferred onto the trenches. Apparent signal difference between the SiO_2 and gap regions can be observed. From the line scan shown in Figure 5c, a strong signal at the gap region is observed for 185 nm SiO_2 trenches, whereas it shows a suppression of signal at the gap region for the 90 nm trenches. The intensity difference is in accordance with the calculation results (see Supporting Information; Figure S6). From the data set, it is clear that the emission intensity for WSe_2 flakes on the SiO_2 substrate and suspended are both governed by the interference instead of doping effect. By using subwavelength gaps, the light emission of 2D materials can be locally engineered to achieve desired patterns with tunable emission strengths. This type of control of photonic properties on 2D materials has not been explored before and is compatible to current optoelectronic techniques.

Besides the substrate effect, the outcoupling can also be tailored by modifying the SiO_2 capping layer on 2D materials (an illustration is shown in inset of Figure 6a). Similar to the

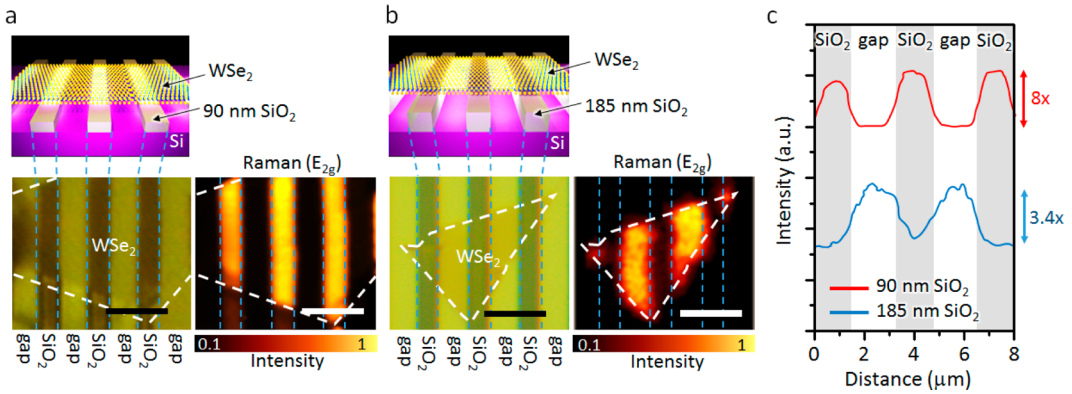

Figure 5. Optical microscope images and Raman mapping of the WSe_2 flakes after transfer onto (a) 90 nm and (b) 185 nm trenches. (c) Intensity line scans corresponding to the mapping in panels a and b. The scale bars in the images are 5 μm.

DOI: 10.1021/nl504632u
Nano Lett. XXXX, XXX, XXX−XXX

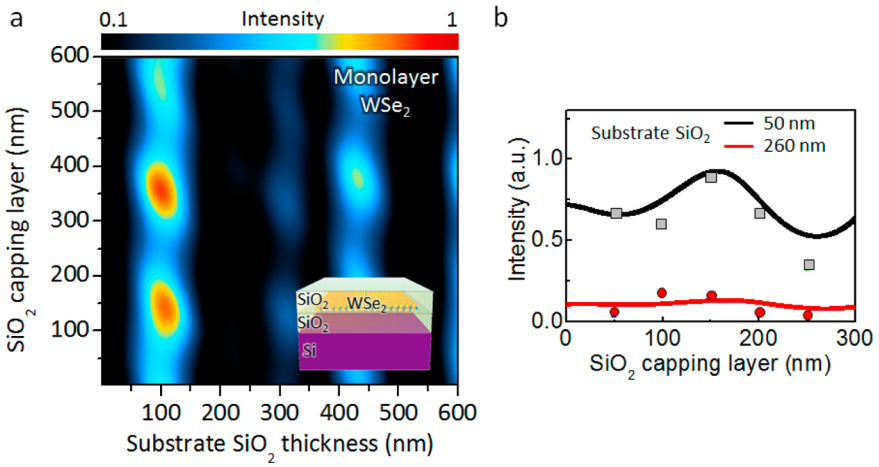

Figure 6. (a) Calculated PL intensity map for WSe_2 as a function of substrate and capping SiO_2 thicknesses. (b) Measured PL intensity for WSe_2 with different thicknesses of SiO_2 capping layers.

substrate effect where the outcoupling strength can be adjusted by changing the substrate thickness, enhanced coupling for a sandwich structure can be achieved by tuning the thickness of the capping SiO_2 layer. Considering the capping layer, a new model considering multiple reflections is built. The full derivation is given in the Supporting Information S7. Figure 6a shows the color map representing the light outcoupling as a function of substrate and capping SiO_2 thicknesses. The emission intensities are maximized at substrate thicknesses of ~100 nm and are diminished at the thicknesses between 150 to 300 nm (Supporting Information S8a), showing a similar trend as that in Figure 2d (substrate effect without capping layer). This indicates that the electrical profile within the dielectric layer is less relevant to the capping thickness, in agreement with the FDTD simulations in Figure 4. On the other hand, the capping layer will determine the boundary conditions of the air-dielectric junction and affect the electrical intensity at the 2D materials (Supporting Information S8b). Experimentally, monolayer WSe_2 flakes are prepared on substrates, and PL is measured as the thickness of the capping layer is increased, as shown in Figure 6b. As expected, the signal shows maximum enhancements as the interference reaches the constructive condition at a substrate thickness of 90 nm and a capping thickness of 150 nm, where the reflection phase is the same as the incident part. This notion allows one to modify the emission intensity from minimum to maximum by simply changing the thickness of the capping layer, which can be a passivation layer for 2D optoelectronics.

In conclusion, via both experimental results and simulations, we have demonstrated ~11 times increase in Raman signal and ~30 times increase in PL intensity of WSe_2 simply by engineering its dielectric surroundings. By modulating the thicknesses of underlying substrates and capping layers, we create a constructive interference between the absorption and emission of light and significantly enhance the outcoupling of WSe_2. Our work proposes an extremely simple way to control the photonic and optoelectronic properties of thin-layer WSe_2, which can be also applied to other direct gap semiconducting two-dimensional materials, such as single-layer MoS_2. Considering the robust and thin body nature of TMDCs, further utilization of outcoupling engineering in 2D materials will make a meaningful contribution to the realization of novel optoelectronic devices, such as 2D materials-based LEDs and solar cells.

Methods. Bulk WSe_2 (Nanosurf) was mechanically exfoliated using the adhesive tape method initially onto a 260 nm SiO_2/Si substrate. Due to the refractive index of WSe_2 and its optical interference with SiO_2/Si, the color contrast between WSe_2 thin layers is the greatest on 260 nm SiO_2/Si. This allows for the flakes of desired thickness to be mapped simply using an optical microscope. For multilayer flakes, atomic force microscopy (DI AFM Nanoscope Dimension 3100) was used to measure their exact thicknesses because it is difficult and inaccurate to figure out the thickness of a multilayer flake just by evaluating its color contrast. Using a poly(methyl methacrylate) (PMMA) membrane as the transfer media, the mapped flakes were then dry-transferred onto substrates with different SiO_2 thicknesses. After removing PMMA with dichloromethane, different thicknesses of SiO_2 were deposited as capping layers using plasma enhanced chemical vapor deposition (Oxford Plasmalab 80 Plus) at 200 °C with a power of 20 W, pressure of 900 mTorr, and precursor flow rates of 800 sccm N_2O and 100 sccm 10% SiH_4 in Ar.

Electron beam lithography is used to define periodic trenches on SiO_2/Si substrates using the PMMA as the resist. Dry etching was then done using CF_4 and O_2 to achieve anisotropic etching. Gas flows of CF_4 and O_2 were set to 90 and 30 sccm, respectively, and an RF power of 300 W was used for etching. After the etching step, PMMA resist was removed in acetone at room temperature.

Raman and PL measurements (Horiba Scientific LabRAM HR 800) were performed in backscattering geometry using a 532 nm laser with 8−80 μW power. A ~0.5 μm spot size was obtained by focusing through a 100× objective. The lowest laser power with a reasonable signal-to-noise ratio (SNR) was chosen to avoid heating effects in WSe_2 thin layers. High-resolution Raman mapping (WITec Alpha 300RA) was also performed with the same laser conditions while scanning the sampling on a piezo stage. Note that the measurement variation/error of the PL/Raman signals in our system is about 10%.

The multiple reflection simulations were performed using LabView and the FDTD simulations were done using RSoft. The refractive index values of WSe_2 at different wavelengths used in these simulations are provided in Supporting

DOI: 10.1021/nl504632u
Nano Lett. XXXX, XXX, XXX−XXX

Information Figure S9. The intensity map in Figure 2C shows distinctive discontinuities between 750 and 800 nm because the refractive index values of WSe_2 used for this calculation show steep variations in this range. The full-wave calculation, which is based on the finite difference method, was used to solve the Maxwell equations in time domain. During this analysis, the resolution of mesh grid was set at 10 nm in the simulation space and a 532 nm plane wave was used as the incident light source.

■ ASSOCIATED CONTENT

Supporting Information

Experimental and calculation details are provided. This material is available free of charge via the Internet at http://pubs.acs.org.

■ AUTHOR INFORMATION

Corresponding Authors

*E-mail: ajavey@eecs.berkeley.edu.
*E-mail: jrhau.he@kaust.edu.sa.

Author Contributions

[▽]These authors contributed equally to this work.

Notes

The authors declare no competing financial interest.

■ ACKNOWLEDGMENTS

The authors acknowledge Joint Center for Artificial Photosynthesis (JCAP), Lawrence Berkeley National Laboratory, for providing access to the Raman and PL measurement tool.

■ REFERENCES

(1) Ross, J. S.; Klement, P.; Jones, A. M.; Ghimire, N. J.; Yan, J.; Mandrus, D. G.; Taniguchi, T.; Watanabe, K.; Kitamura, K.; Yao, W.; Cobden, D. H.; Xu, X. *Nat. Nanotechnol.* **2014**, *9*, 268−72.

(2) Pospischil, A.; Furchi, M. M.; Mueller, T. *Nat. Nanotechnol.* **2014**, *9*, 257−61.

(3) Tsai, D. S.; Liu, K. K.; Lien, D. H.; Tsai, M. L.; Kang, C. F.; Lin, C. A.; Li, L. J.; He, J. H. *ACS Nano* **2013**, *7*, 3905−11.

(4) Tsai, D. S.; Lien, D. H.; Tsai, M. L.; Su, S. H.; Chen, K. M.; Ke, J. J.; Yu, Y. C.; Li, L. J.; He, J. H. *IEEE J. Sel. Top. Quantum Electron.* **2014**, *20*, 3800206.

(5) Baugher, B. W.; Churchill, H. O.; Yang, Y.; Jarillo-Herrero, P. *Nat. Nanotechnol.* **2014**, *9*, 262−7.

(6) Desai, S. B.; Seol, G.; Kang, J. S.; Fang, H.; Battaglia, C.; Kapadia, R.; Ager, J. W.; Guo, J.; Javey, A. *Nano Lett.* **2014**, *14*, 4592−7.

(7) Splendiani, A.; Sun, L.; Zhang, Y. B.; Li, T. S.; Kim, J.; Chim, C. Y.; Galli, G.; Wang, F. *Nano Lett.* **2010**, *10*, 1271−1275.

(8) Hui, Y. Y.; Liu, X.; Jie, W.; Chan, N. Y.; Hao, J.; Hsu, Y. T.; Li, L. J.; Guo, W.; Lau, S. P. *ACS Nano* **2013**, *7*, 7126−31.

(9) Berciaud, S.; Ryu, S.; Brus, L. E.; Heinz, T. F. *Nano Lett.* **2009**, *9*, 346−52.

(10) Sercombe, D.; Schwarz, S.; Del Pozo-Zamudio, O.; Liu, F.; Robinson, B. J.; Chekhovich, E. A.; Tartakovskii, I. I.; Kolosov, O.; Tartakovskii, A. I. *Sci. Rep.* **2013**, *3*, 3489.

(11) Buscema, M.; Steele, G. A.; van der Zant, H. S. J.; Castellanos-Gomez, A. *Nano Res.* **2014**, *7*, 561−571.

(12) Mak, K. F.; Lee, C.; Hone, J.; Shan, J.; Heinz, T. F. *Phys. Rev. Lett.* **2010**, *105*, 13.

(13) Scheuschner, N.; Ochedowski, O.; Kaulitz, A. M.; Gillen, R.; Schleberger, M.; Maultzsch, J. *Phys. Rev. B* **2014**, *89*, 125406.

(14) Balanis, C. A. *Antenna theory: analysis and design*, 3rd ed.; John Wiley: Hoboken, NJ, 2005.

(15) Fang, H.; Bechtel, H. A.; Plis, E.; Martin, M. C.; Krishna, S.; Yablonovitch, E.; Javey, A. A. *Proc. Natl. Acad. Sci. U.S.A.* **2013**, *110*, 11688−91.

(16) Li, S. L.; Miyazaki, H.; Song, H.; Kuramochi, H.; Nakaharai, S.; Tsukagoshi, K. *ACS Nano* **2012**, *6*, 7381−8.

(17) Yoon, D.; Moon, H.; Son, Y. W.; Choi, J. S.; Park, B. H.; Cha, Y. H.; Kim, Y. D.; Cheong, H. *Phys. Rev. B* **2009**, *80*, 125422.

(18) Liu, Y.; Cheng, R.; Liao, L.; Zhou, H.; Bai, J.; Liu, G.; Liu, L.; Huang, Y.; Duan, X. *Nat. Commun.* **2011**, *2*, 579.

(19) Lin, J. D.; Li, H.; Zhang, H.; Chen, W. *Appl. Phys. Lett.* **2013**, *102*, 203109.

(20) Furchi, M.; Urich, A.; Pospischil, A.; Lilley, G.; Unterrainer, K.; Detz, H.; Klang, P.; Andrews, A. M.; Schrenk, W.; Strasser, G.; Mueller, T. *Nano Lett.* **2012**, *12*, 2773−2777.

(21) Henrie, J.; Kellis, S.; Schultz, S.; Hawkins, A. *Opt. Express* **2004**, *12*, 1464−9.

(22) Roddaro, S.; Pingue, P.; Piazza, V.; Pellegrini, V.; Beltram, F. *Nano Lett.* **2007**, *7*, 2707−10.

(23) Casiraghi, C.; Hartschuh, A.; Lidorikis, E.; Qian, H.; Harutyunyan, H.; Gokus, T.; Novoselov, K. S.; Ferrari, A. C. *Nano Lett.* **2007**, *7*, 2711−7.

(24) Fang, H.; Battaglia, C.; Carraro, C.; Nemsak, S.; Ozdol, B.; Kang, J. S.; Bechtel, H. A.; Desai, S. B.; Kronast, F.; Unal, A. A.; Conti, G.; Conlon, C.; Palsson, G. K.; Martin, M. C.; Minor, A. M.; Fadley, C. S.; Yablonovitch, E.; Maboudian, R.; Javey, A. *Proc. Natl. Acad. Sci. U.S.A.* **2014**, *111*, 6198−202.

(25) Huang, J. K.; Pu, J.; Hsu, C. L.; Chiu, M. H.; Juang, Z. Y.; Chang, Y. H.; Chang, W. H.; Iwasa, Y.; Takenobu, T.; Li, L. J. *ACS Nano* **2014**, *8*, 923−930.

(26) Koh, Y. K.; Bae, M. H.; Cahill, D. G.; Pop, E. *ACS Nano* **2011**, *5*, 269−74.

(27) Schmid, T.; Opilik, L.; Blum, C.; Zenobi, R. *Angew. Chem., Int. Ed.* **2013**, *52*, 5940−5954.

DOI: 10.1021/nl504632u
Nano Lett. XXXX, XXX, XXX−XXX

Supplementary Information for

Engineering Light Outcoupling in 2D Materials

Der-Hsien Lien[1,2,3,4†], Jeong Seuk Kang[1,2†], Matin Amani[1,2], Kevin Chen[1,2], Mahmut Tosun[1,2], Hsin-Ping Wang[1,2,3,4], Tania Roy[1,2], Michael S. Eggleston[1], Ming C. Wu[1], Madan Dubey[5], Si-Chen Lee[4], Jr-Hau He[3] and Ali Javey[1,2*]*

[1]*Electrical Engineering and Computer Sciences, University of California, Berkeley, CA 94720*

[2]*Materials Sciences Division, Lawrence Berkeley National Laboratory, Berkeley, CA 94720*

[3]*Computer, Electrical and Mathematical Sciences and Engineering (CEMSE) Division, King Abdullah University of Science & Technology (KAUST), Thuwal 23955-6900, Saudi Arabia*

[4]*Department of Electrical Engineering, Institute of Electronics Engineering, National Taiwan University, Taipei 10617, Taiwan, ROC*

[5]*Sensors and Electron Devices Directorate, US Army Research Laboratory, Adelphi MD 20783, USA*

[†]*These authors contributed equally to this work.*

[*]*E-mail: ajavey@eecs.berkeley.edu; jrhau.he@kaust.edu.sa*

Supplementary Figure S1 | Reversible Raman/PL Intensity changes.

Using PMMA as the transfer medium, the flakes were transferred onto substrates with different SiO_2 thicknesses in the following order: 260 nm, 90nm, 185 nm, 90nm, and 260 nm. As shown in figure S1a and S1b, the PL and Raman spectra of both monolayer and bilayer WSe_2 on 90 nm and 260 nm have similar intensity, peak position, and FWHM, regardless of preceding transfer stages or substrates. This demonstrates the repeatability and reversibility of the proposed outcoupling engineering method.

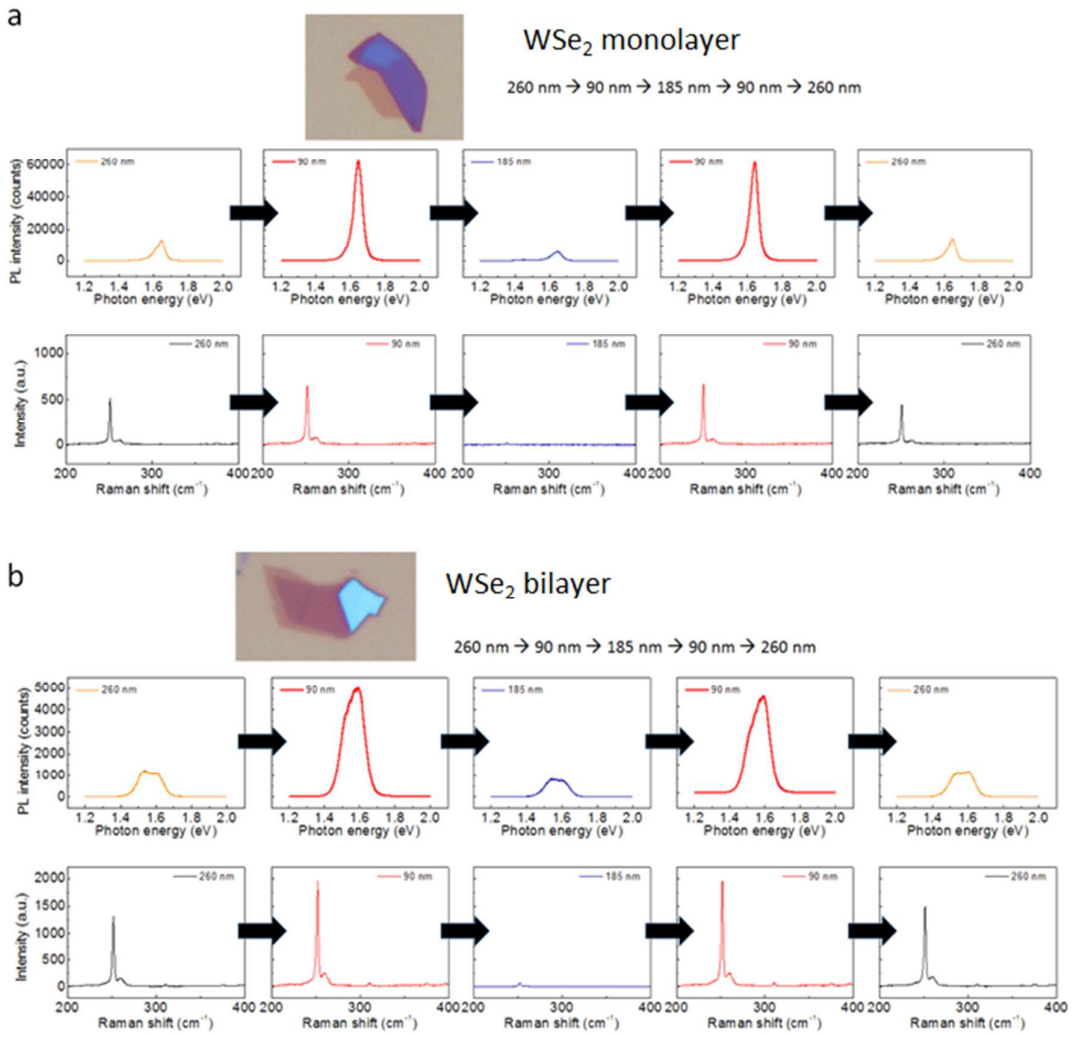

Figure S1 | Reversible Raman/PL Intensity changes. a, PL and Raman spectra of a monolayer WSe_2 measured initially on 260 nm SiO_2 and subsequently on 90 nm, 185 nm, 90 nm, and 260 nm SiO_2 to demonstrate the reversibility of our outcoupling engineering method. **b,** PL and Raman spectra of a bilayer WSe_2 also measured initially on 260 nm SiO_2 and subsequently on 90 nm, 185 nm, 90 nm, and 260 nm SiO_2 for the reversibility demonstration. In both cases, the PL and Raman peak positions and intensities on the same thickness of SiO_2 remain unchanged after the flakes were transferred onto different substrates via dry transfer method.

Supplementary Figure S2 | Derivation of the 4 layer-multiple reflection model.

The four media shown in figure S2, namely PMMA, WSe_2, SiO_2 and Si, are denoted as $\tilde{n}_0$, $\tilde{n}_1$, $\tilde{n}_2$ and $\tilde{n}_3$, respectively. Figure S2 illustrates the trajectories of laser light upon entering different media, which the Fresnel transmittance and reflection coefficients at each interface are highly dependent on. $r_{ij} = (\tilde{n}_i - \tilde{n}_j)/(\tilde{n}_i + \tilde{n}_j)$ and $t_{ij} = 2\tilde{n}_i / (\tilde{n}_i + \tilde{n}_j)$ as a beam reaches the interface ij between media i and j and propagates from medium i to j. The two reflection coefficients r_{ij} and r_{ji} from each side of the interface ij have the following relationship: $r_{ij} = -r_{ji}$. Due to the optical reversibility principle, the following relationship also holds true: $t_{ij}t_{ji} - r_{ij}\ r_{ji} = 1$. In addition, there exists phase differences for path *x* in WSe_2 and the whole medium j, which can be expressed as $\beta_x = 2\pi\tilde{n}_i x/\lambda$ and $\beta_j = 2\pi\tilde{n}_j d_j/\lambda$ (j = 1 or 2), respectively. Here, λ is the wavelength of the excitation or scattering light and d_j is the thickness of medium j.

1. The effective reflection coefficient at the WSe_2/SiO_2 interface, including multiple reflections in the lower SiO_2 layer is first calculated. The schematic demonstrating the reflections is shown in Figure S2b and individual components can be written as:

$b_1 = r_{12}$

$b_2 = t_{12} \cdot e^{-i\beta_2} \cdot r_{23} \cdot e^{-i\beta_2} \cdot t_{21} = t_{12}t_{21}t_{23}e^{-2i\beta_2}$

$b_3 = t_{12} \cdot e^{-i\beta_2} \cdot r_{23} \cdot e^{-i\beta_2} \cdot r_{21} \cdot e^{-i\beta_2} \cdot r_{23} \cdot e^{-i\beta_2} \cdot t_{21} = b_2 \cdot (r_{21}r_{23}e^{-2i\beta_2})$

$b_4 = t_{12} \cdot e^{-i\beta_2} \cdot r_{23} \cdot e^{-i\beta_2} \cdot r_{21} \cdot e^{-i\beta_2} \cdot r_{23} \cdot e^{-i\beta_2} \cdot r_{21} \cdot e^{-i\beta_2} \cdot r_{23} \cdot e^{-i\beta_2} \cdot t_{21}$

$= b_2 \cdot (r_{21}r_{23}e^{-2i\beta_2})^2$

...

$b_n = b_2 \cdot (r_{21}r_{23}e^{-2i\beta_2})^{n-2}$

$$r' = r_{12} + t_{12}t_{21}t_{23}e^{-2i\beta_2} \cdot \sum_{n=0}^{\infty} \left(r_{21}r_{23}e^{-2i\beta_2}\right)^n = r_{12} + \frac{t_{12}t_{21}t_{23}e^{-2i\beta_2}}{1 - r_{21}r_{23}e^{-2i\beta_2}}$$

Applying the relationships $r_{21} = -r_{12}$ and $t_{12}t_{21} = 1 - {r_{12}}^2$,

$$r' = r_{12} + \frac{(1-{r_{12}}^2)r_{23}e^{-2i\beta_2}}{1+r_{12}r_{23}e^{-2i\beta_2}} = \frac{r_{12}+r_{23}e^{-2i\beta_2}}{1+r_{12}r_{23}e^{-2i\beta_2}} ----- (1)$$

2. The total amplitude of absorption/excitation light at depth x in WSe_2 is demonstrated below. The schematic corresponding to this derivation is shown in figure S2c and the individual components can be written as:

$c_1 = t_{01} \cdot e^{-i\beta_x}$

$c_2 = t_{01} \cdot e^{-i\beta_1} \cdot r' \cdot e^{-i(\beta_1-\beta_x)} = t_{01}r'e^{-i(2\beta_1-\beta_x)}$

$c_3 = t_{01} \cdot e^{-i\beta_1} \cdot r' \cdot e^{-i\beta_1} \cdot r_{10} \cdot e^{-i\beta_x} = c_1(r'r_{10}e^{-2i\beta_1})$

$c_4 = t_{01} \cdot e^{-i\beta_1} \cdot r' \cdot e^{-i\beta_1} \cdot r_{10} \cdot e^{-i\beta_1} \cdot r' \cdot e^{-i(\beta_1-\beta_x)} = c_2(r'r_{10}e^{-2i\beta_1})$

...

$c_{2n+1} = c_1(r'r_{10}e^{-2i\beta_1})^n$

$c_{2n+2} = c_2(r'r_{10}e^{-2i\beta_1})^n$

Therefore, the total amplitude of the absorption/excitation light at depth x in WSe_2 is:

$$I_{ex}(x) = \sum_{n=0}^{\infty}\left(t_{01}e^{-i\beta_x} \cdot (r'r_{10}e^{-2i\beta_1})^n + t_{01}r'e^{-i(2\beta_1-\beta_x)} \cdot (r'r_{10}e^{-2i\beta_1})^n\right)$$

$$= t_{01} \cdot \frac{e^{-i\beta_x} + r'e^{-i(2\beta_1-\beta_x)}}{1+r'r_{01}e^{-2i\beta_1}} ----- (2)$$

3. The amplitude of emission/scattering light from depth x in WSe_2 is demonstrated here. The schematic corresponding to the derivation is shown in figure S2d and the individual components can be written as:

$d_1 = t_{10} \cdot e^{-i\beta_x}$

$d_2 = e^{-i(\beta_1-\beta_x)} \cdot r' \cdot e^{-i\beta_1} \cdot t_{10} = t_{10}r'e^{-i(2\beta_1-\beta_x)}$

$d_3 = e^{-i\beta_x} \cdot r_{10} \cdot e^{-i\beta_1} \cdot r' \cdot e^{-i\beta_1} \cdot t_{10} = d_1(r'r_{10}e^{-2i\beta_1})$

$d_4 = e^{-i(\beta_1-\beta_x)} \cdot r' \cdot e^{-i\beta_1} \cdot r_{10} \cdot e^{-i\beta_1} \cdot r' \cdot e^{-i\beta_1} \cdot t_{10} = d_2(r'r_{10}e^{-2i\beta_1})$

...

$$d_{2n+1} = d_1(r'r_{10}e^{-2i\beta_1})^n$$

$$d_{2n+2} = d_2(r'r_{10}e^{-2i\beta_1})^n$$

Therefore, the amplitude of emission/scattering light from depth x in WSe_2 is:

$$I_{em}(x) = \sum_{n=0}^{\infty}\left(t_{10}e^{-i\beta_x}\cdot(r'r_{10}e^{-2i\beta_1})^n + t_{10}r'e^{-i(2\beta_1-\beta_x)}\cdot(r'r_{10}e^{-2i\beta_1})^n\right)$$

$$= t_{10}\cdot\frac{e^{-i\beta_x} + r'e^{-i(2\beta_1-\beta_x)}}{1 + r'r_{01}e^{-2i\beta_1}} - - - - - (3)$$

Based on this model, all parameters are set according to the experiment conditions we used. The outcoupling intensity for the WSe_2 flakes can then be expressed as:

$$I = \int_0^d |E_{\mathrm{ex}}(x)E_{\mathrm{em}}(x)|^2 dx$$

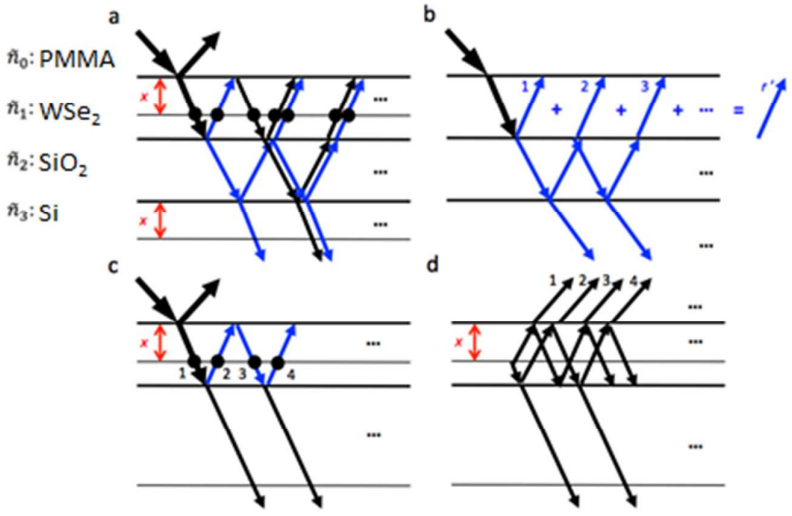

Figure S2 | Derivation of the 4 layer-multiple reflection model. Schematics showing **a,** overall trajectories of the incident light in four media denoted as $\tilde{n}_0$ (PMMA), $\tilde{n}_1$ (WSe_2), $\tilde{n}_3$ (SiO_2) and $\tilde{n}_4$ (Si). **b,** Effective reflection at the WSe_2/SiO_2 interface. **c,** Amplitudes of the absorption/excitation light at depth x in WSe_2. **d,** Amplitudes of the emission/scattering light at depth x in WSe_2

Supplementary Figure S3 | Examining the contribution of absorption and emission.

To further explain light outcoupling using the substrate, we separate the substrate effect in terms of absorption and emission parts. Absorption by the flakes can be expressed as: $\int_0^d |E_{\mathrm{ab}}(x))|^2 dx$, and emission can be expressed as: $\int_0^d |E_{\mathrm{em}}(x)|^2 dx$, where $E_{\mathrm{ab}}(x)$ and $E_{\mathrm{em}}(x)$ are the electric field amplitudes within the flakes and light emitting out the flakes, respectively. The results are shown in Figures S3a and S3b. The improved outcoupling is attributed to a combined effect of enhanced absorption and emission modulated by substrate-induced interference. Since the incident light is fixed (532 nm), the amount of light absorption is mainly governed by the Fabry-Perot interference which shows a periodic variance with SiO_2 thickness. On the other hand, the strength of emission shows an irregular profile due to a combined effect of the substrate interference and the wavelength-dependent refractive index. Figure S3c and S3d correspond to the PL emission (752 nm) and Raman scattering wavelengths (532 nm) of WSe_2. Enhanced outcoupling occurs when both absorption and emission meet constructive interference, which yields ~11 times enhancement of PL and 30 times enhancement of Raman compared to those in destructive cases.

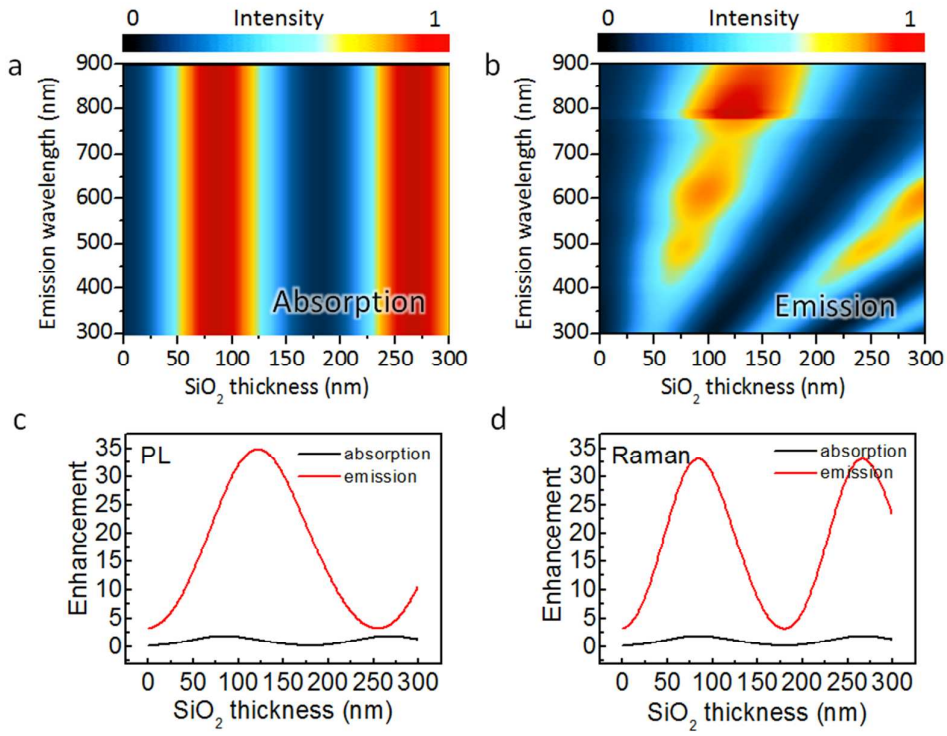

Figure S3 | Examining the contribution of absorption and emission to overall outcoupling. a, The absorption of WSe_2 as a function of incident wavelengths. **b,** The emission intensity of WSe_2 as a function of emission wavelengths. **c,** Separating the absorption and emission parts for the PL of WSe_2 as a function of emission wavelengths. **d,** Separating the excitation and scattering parts for the Raman of WSe_2 as a function of emission wavelengths.

Supplementary Figure S4 | PL intensity as a function of WSe_2 NL.

The PL intensity as a function of SiO_2 thickness and WSe_2 NL is shown in Figure S4a. The PL result is similar to that of Raman results. As shown in Figures S4b and S4c, the PL intensity shows the highest response when the flake sits on 90 nm substrates for 2L, 3L and 4L WSe_2 flakes. However, due to a direct to indirect transition with increased NL, the signal shows a dramatic decrease as the NL of flake increases from 2L to 4L. Both of the substrate effect and electronic band structure needs to considered for PL outcoupling response, and a direct to indirect transition with increasing NL dominates the PL intensity rather than the substrate effect

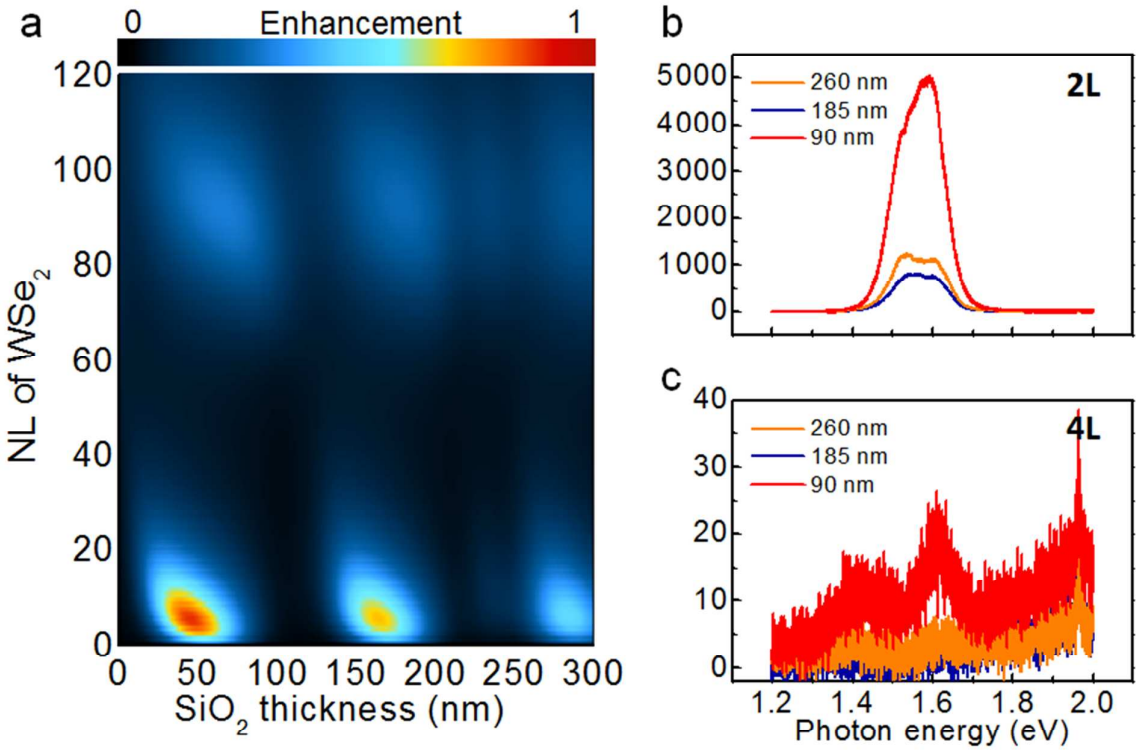

Figure S4 | Thickness-dependent PL intensities for WSe_2 as a function of NL. **a,** Calculation of the thickness-dependent PL intensities for WSe_2. **b,** Experimental results of the PL profile of 2-layer WSe_2 on different SiO_2 substrates. **c,** Experimental results of the PL profile of 4-layer WSe_2 on different SiO_2 substrates.

Supplementary Figure S5 | An example of Substrate-enhanced Raman spectroscopy.

Figure S5 shows the Raman mapping of WSe_2 flakes exfoliated on 90 nm, 185 nm and 260 nm SiO_2/Si substrates. From the images it clearly shows that the flakes on 90 nm and 260 nm substrates exhibits stronger responses than on a 185 nm substrate. The results are in agreement with the calculation results shown in Figure 1d. It demonstrates a new strategy, namely, substrate-enhanced Raman spectroscopy, to achieve higher sensitivity for 2D materials characterization simply by adjusting the substrate.

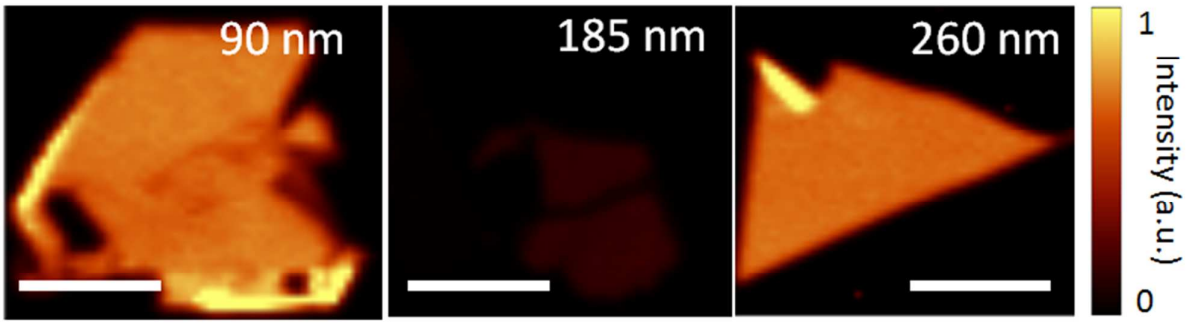

Figure S5 | An example of Substrate-enhanced Raman spectroscopy. The Raman mapping of monolayer WSe_2 flakes on different thicknesses of SiO_2/Si substrates. The scale bar is 5 μm.

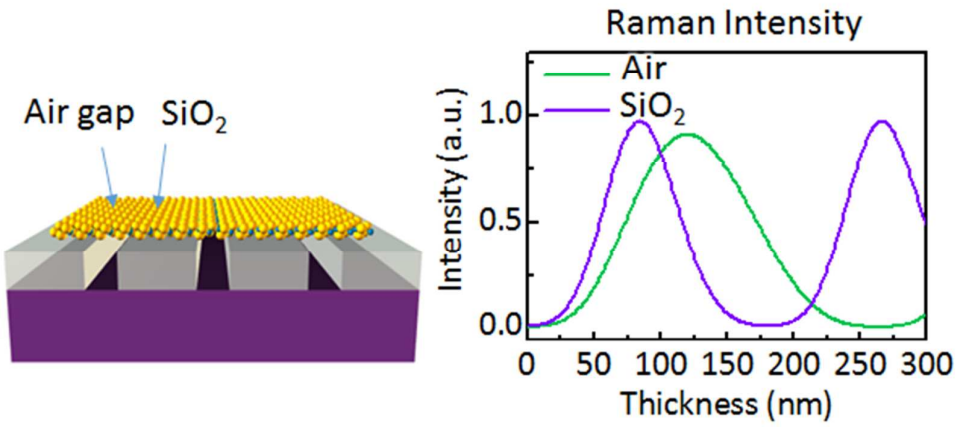

Figure S6 | The Raman intensity of WSe_2 on trenches. Raman intensity of WSe_2 as a function of underlying SiO_2 thickness and gap depth using the multiple reflection model.

Supplementary Figure S7| Derivation of the 5 layer-multiple reflection model.

The five media shown in figure S7 are assigned an index i, and their corresponding (complex) refractive indices are denoted as $\tilde{n}_i$, where i = 0, 1, 2, 3 and 4 for air, capping-layer SiO_2, WSe_2, SiO_2 and Si, respectively. The derivation concept is the same as that of the four layer model. The difference is that we introduce an effective transmission coefficient *t'* at the capping-layer SiO_2/WSe_2 interface and an effective reflection coefficient *r''* at the WSe_2/capping layer SiO_2 interface.

1. The effective reflection coefficient *r''* at the WSe_2/capping layer SiO_2 interface is to consider the multiple reflection within the capping SiO_2 layer in order to simplify the absorption model. The schematic is shown in figure S7a and the individual components can be written as:

$a_1 = r_{21}$

$a_2 = t_{21} \cdot e^{-i\beta_1} \cdot r_{10} \cdot e^{-i\beta_1} \cdot t_{12}$

$a_3 = a_2 \cdot (r_{10} r_{12} e^{-2i\beta_1})$

...

$a_n = a_2 \cdot (r_{10} r_{12} e^{-2i\beta_1})^{n-2}$

Therefore, the total amplitude is:

$$r'' = r_{21} + t_{21} t_{12} r_{10} e^{-2i\beta_1} \cdot \sum_{n=0}^{\infty} \left(r_{10} r_{12} e^{-2i\beta_1}\right)^n = \left(r_{21} + r_{10} e^{-2i\beta_1}\right) \Big/ \left(\frac{t_{12} t_{21} t_{23} e^{-2i\beta_2}}{1 - r_{21} r_{23} e^{-2i\beta_2}}\right)$$

$$-----(1)$$

2. The effective reflection coefficient *r'* at the WSe_2/SiO_2 interface is the same as the model described above except that the denotation numbers should be corrected.

$$r' = \frac{r_{23} + r_{34} e^{-2i\beta_3}}{1 + r_{23} r_{34} e^{-2i\beta_3}} ----- (2)$$

3. The schematic of the absorption/excitation light is shown in figure S7b. The total amplitude of absorption/excitation light at depth x in WSe_2 is expressed as

$b_1 = t_{01} \cdot e^{-i\beta_1} \cdot t_{12} \cdot e^{-i\beta_x}$

$b_2 = t_{01} \cdot e^{-i\beta_1} \cdot t_{12} \cdot e^{-i\beta_2} \cdot r' \cdot e^{-i(\beta_2-\beta_x)}$

$b_3 = b_1(r'r''e^{-2i\beta_2})$

$b_4 = b_2(r'r''e^{-2i\beta_2})$

...

$b_{2n+1} = b_1(r'r''e^{-2i\beta_2})^n$

$b_{2n+2} = b_2(r'r''e^{-2i\beta_2})^n$

Therefore, the total amplitude of the absorption/excitation light at depth x in WSe_2 is:

$$E_{\mathrm{ab}}(x) = t_{01} \cdot \frac{e^{-i\beta_x} + r'e^{-i(2\beta_2-\beta_x)}}{1 - r'r''e^{-2i\beta_2}} \quad -----(3)$$

4. To simplify the model, we introduce an effective transmission coefficient *t'* at the capping-layer SiO_2/WSe_2 interface:

$c_1 = t_{21} \cdot e^{-i\beta_1} \cdot t_{10}$

$c_2 = t_{21} \cdot e^{-i\beta_1} \cdot r_{10} \cdot e^{-i\beta_1} \cdot r_{12} \cdot e^{-i\beta_1} \cdot t_{10}$

$c_3 = c_2(r_{10}r_{12}e^{-2i\beta_1})$

...

Therefore, the total amplitude is:

$$t' = t_{21}t_{10}e^{-i\beta_1} \cdot \sum_{n=0}^{\infty}\left(r_{10}r_{12}e^{-2i\beta_1}\right)^n = \frac{t_{10}t_{21}e^{-i\beta_2}}{1 - r_{10}r_{12}e^{-2i\beta_2}} \quad -----(4)$$

5. The schematic of the emission/scattering light is shown in S7d. The total amplitude of absorption/excitation light at depth x in WSe_2 is expressed as

$d_1 = t' \cdot e^{-i\beta_x}$

$d_2 = e^{-i(\beta_2-\beta_x)} \cdot r' \cdot e^{-i\beta_2} \cdot t' = r't'e^{-i(2\beta_2-\beta_x)}$

$d_3 = d_1(r'r_{21}e^{-2i\beta_2})$

$d_4 = d_2(r'r_{21}e^{-2i\beta_2})$

...

$d_{2n+1} = d_1(r'r_{21}e^{-2i\beta_2})^n$

$d_{2n+2} = d_2(r'r_{21}e^{-2i\beta_2})^n$

Therefore, the amplitude of emission/scattering light from depth x in WSe_2 is:

$$I_{\mathrm{em}}(x) = t' \cdot \frac{e^{-i\beta_x} + r'e^{-i(2\beta_2-\beta_x)}}{1 + r'r_{12}e^{-2i\beta_1}} - - - - - (5)$$

The same as the four-layer model, the outcoupling intensity for the WSe_2 flakes is accordingly given by

$$I = \int_0^d |E_{\mathrm{ab}}(x)E_{\mathrm{em}}(x)|^2 dx$$

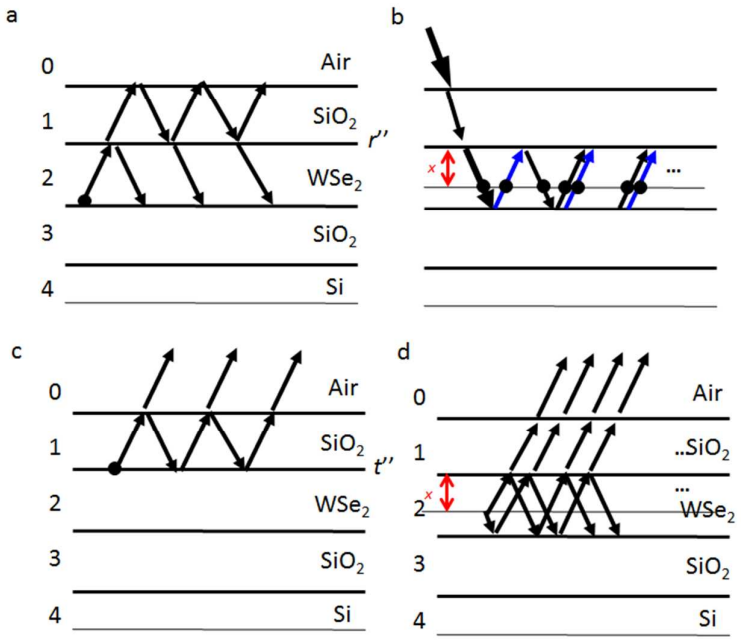

Figure S7 | Derivation of the 5 layer-multiple reflection model. Schematics showing **a,** the effective reflection coefficient *r''* at the WSe_2/capping layer SiO_2 interface. **b,** Amplitudes of the

absorption/excitation light at depth x in WSe_2. **c,** An effective transmission coefficient t' at the capping-layer SiO_2/WSe_2 interface. **d,** Amplitudes of the emission/scattering light at depth x in WSe_2

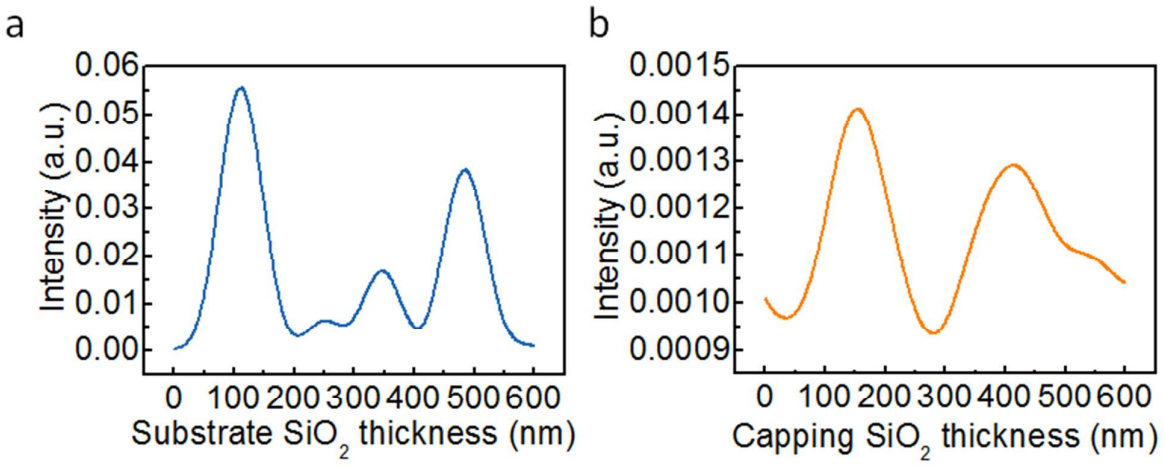

Figure S8 | Averaging the intensity values in Figure 6. Average intensity as a function of **a,** substrate SiO_2 thickness and **b,** capping SiO_2 thickness with thicknesses ranging from 1 to 600 nm.

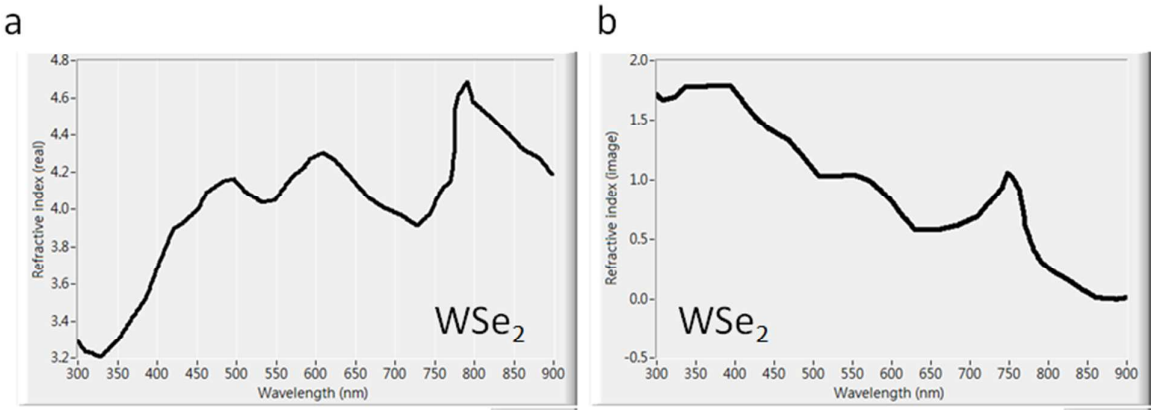

Figure S9 | Refractive index of WSe_2. The refractive index of WSe_2 as a function of wavelength used for the simulations: (a) real part and (b) imaginary part.[1]

Reference

(1) Beal, R.; Liang, W. Y.; Hughes, H. P. J. Phys. C: Solid State Phys. 1976, 9, 2449.